Journal of Ovonic Research Vol. 20, No. 2, March - April 2024, p. 143 - 153

Synthesis and Exploring structural, magnetic, morphology and optical properties of $La_{2-x}Al_xCuO_4$ ($0 \leq x \leq 0.25$) perovskite nanoparticles by microwave-assisted combustion method

S. Yuvaraj[a], P. Aji Udhaya[b], S. Deepa, M. Sundararajan[d], R. Jothiramalingam [e *], H. Al-Lohedan[e], H. Al-Sigh[e], A. A. Nazeer[f]

[a]*Department of Physics, Vel Tech Rangarajan Dr. Sagunthala R&D Institute of Science and Technology, Vel Nagar, Avadi, Chennai-600 062, Tamil Nadu, India*
[b]*Department of Physics, Holy Cross College (Autonomous), Nagercoil, Affiliated to Manonmaniam Sundaranar University Tirunelveli, Tamil Nadu, India*
[c]*Department of Chemistry, School of Basic Sciences, Vels Institute of Science Technology and Advanced Studies, Pallavaram, Chennai 600 117*
[d]*PG & Research Department of Physics, Paavendhar College of Arts & Science, M.V. South, Thalaivasal, Salem, Tamil Nadu 636 121, India*
[e]*Department of Chemistry, College of Science, King Saud University, P.O.Box. 2455, Riyadh 11451, Saudi Arabia*
[f]*College of Pharmacy, Kangwon National University, Chuncheon, Gangwo—24341, Republic of Korea*

La_2CuO_4 perovskite nanoparticles doped with aluminum were synthesized through the microwave-assisted combustion technique. Comprehensive studies on the structural, magnetic optical, functional and morphological properties were conducted using various techniques, including XRD, EDX, VSM, DRS-UV, FT-IR and FESEM respectively, .The XRD patterns of pristine La_2CuO_4 and Al-doped La_2CuO_4 unequivocally validated the exclusive development of a perovskite structure, devoid of any impurities. Nevertheless, the augmentation in Al^{3+} content (x = 0–0.25) induced a noteworthy phase shift from orthorhombic to cubic configuration. The average crystallite dimensions spanned from 54 to 41 nm. Distinct FT-IR bands at approximately 687 and 434 cm^{-1} were intricately linked to the La-O and Cu-O stretching modes inherent to the orthorhombic La_2CuO_4 phase. The energy gap determined through the Kubelka–Munk (K–M) methodology, experienced an elevation concomitant with the heightened Al^{3+} content (1.67–1.72 eV), attributable to quantum confinement phenomena. Within the $La_{2-x}Al_xCuO_4$ (x = 0 to 0.25) system, the genesis of nanoscaled crystallized grains, interspersed with pores resulting from the amalgamation of grains, was evident. Analysis of hysteresis curves unveiled the emergence of soft ferromagnetic behavior at ambient temperature.

(Received November 13, 2023; Accepted March 7, 2024)

Keywords: La_2CuO_4 nanoparticls, Perovskite, Pore-wall grains, Band gap, Soft ferromagnetic

1. Introduction

The peculiar physio-chemical characteristics of nanomaterials are a result of their small size. They become popular as a result, being used in numerous applications such as photodegradation, catalysis, and more [1-4]. La_2CuO_4 is a perovskite-like substance that has gained attention for its wide range of potential uses in the energy and environmental fields, including ceramic fuel cell, electrode materials for oxidation and reduction reaction, catalysis, gas sensors, superconducting catalysis, and superconductors [5,6]. Materials based on lanthanum (La^{3+}) exhibit greater carbon oxidation activity. The increased lattice mobility of O^{2-} ions may be

* Corresponding author: rjothiram@gmail.com
https://doi.org/10.15251/JOR.2024.202.143

related to the function of perovskites as oxidation catalysts. The movement of ions in a surface-directed manner can create additional catalytic site for the oxidation of carbonaceous materials [7-9]. The rock-salt (sodium chloride) structure, represented by AO, and the ABO_3 perovskite structure are arranged in alternating layers to create the A_2BO_4 structure, as exemplified by La_2CuO_4. In this arrangement, the A-site cation corresponds to a trivalent metal ion, exhibiting nine-fold coordination, while the B-site cation represents a divalent metal ion, displaying octahedral coordination [10].

LCO, or La_2CuO_4, is a anti-ferromagnetic semiconductor (p-type) that exhibits structural variations between tetragonal and orthorhombic forms under the influence of doping, pressure, temperature [11]. This metal oxide displays three primary structural phases with P42/ncmBmab, and I4/mmm symmetry, namely: (i) High Temperature Tetragonal (HTT): At higher temperatures, the tetragonal phase (P42/ncm symmetry) of LCO becomes prominent (ii) Low Temperature Orthorhombic (LTO): LCO can also exist in a low-temperature orthorhombic phase (Bmab symmetry) (iii) Low Temperature Tetragonal (LTT): At low temperatures, LCO adopts a tetragonal structure (I4/mmm symmetry) [12,13].

The La_2CuO_4 nanoparticles were synthesized using a chemical and physical techniques such as hydrothermal [14], combustion [15], sol-gel [16], solid state [17] and co-precipitation [18] techniques. Velasquez et al. Synthesized La_2CuO_4 using glycine and used it to convert glycerol to hydroxyacetone using the self-combustion method [19-20]. However, there aren't many publications on the microwave combustion method used to prepare La_2CuO_4, which was then evaluated for its catalytic activity in glycerol oxidation, exploring its potential applications in catalysis.

2. Experimental

2.1. Materials

The chemicals employed in the study, including lanthanum nitrate, aluminum nitrate, copper nitrate, and L-alanine, were of analytical grade (99.9%) and were procured from SD Fine Chemicals, India. These chemicals were used without any additional purification. During the sample preparation process, double-distilled water was utilized.

2.2. Preparation of $La_{2-x}Al_xCuO_4$ perovskite nanoparticles

In order to create a homogenous solution, the ingredients were dissolved in deionized water at the desired proportion. L-alanine served as the fuel for the reaction, and the precursors' nitrates acted as the oxidizers. In accordance with propellant chemistry theory, the ratio of fuel to oxidizer (F/O) was set to 1. After that, the sample was heated using hot air oven 110˚C for 60 minutes was used to expose the homogenous solution. The solution initially boiled, underwent dehydration, breakdown, and gas evolution, producing a black, fluffy powder. The $La_{2-x}Al_xCuO_4$ final products (with x varying from 0 to 0.25) were obtained by calcining the powder at 750°C for a duration of 90 minutes. The samples created with $La_{2-x}Al_xCuO_4$ (x = 0 to 0.25)at stoichiometric concentrations of x = 0, 0.05, 0.15, and 0.25 were designated as a, b, c, and d, respectively.

2.3. Characterization

The crystalline phase of the powders was analyzed using an X-ray diffractometer (Rigaku Model Smartlab 3 kW X-ray diffractometer) within the 2θ range of 20-80°, employing Cu Kα radiation with a wavelength of 1.5406 Å. This analysis allowed for the determination of the phases present in the formed powders.

Surface functional groups were analyzed using the Thermo Scientific Nicolet 10 OMNI FTIR spectrophotometer, capturing spectra in the wavenumber region of 4000 - 400 cm^{-1}. This allowed for the identification of the surface functional groups present in the samples. Morphological observations were conducted using a HITACHI S4800 HR-field scanning electron microscope (HR-SEM) (EDX) system for elemental composition analysis. Magnetic measurements were carried out using a PMC Micro Mag 3900 model vibrating sample magnetometer (VSM).

3. Result and discussion

3.1. X-ray diffraction analysis

Figure 1 displays the XRD patterns of the Al-doped La_2CuO_4perovskite nanoparticles. The undoped La_2CuO_4 exhibits a distinct single orthorhombic perovskite phase characterized by the Bmab space group (JCPDS No. 88-0940). It is clear from this that only one La_2CuO_4perovskite phase needs to be prepared using the chosen combustion method, followed by calcination at 750˚C for 90 minutes. The XRD pattern exhibits characteristic peaks at specific 2θ values, namely 24.32, 27.13, 31.04, 33.07, 33.38, 41.23, 41.67, 43.45, 47.76, 53.86, 54.45, 55.85, 58.04, 64.82, 65.31, 69.60, 70.00, 75.28, 76.50, and 78.54. These peaks correspond to the crystallographic planes (111), (004), (113), (020), (200), (006), (115), (204), (220), (206), (117), (224), (133), (226), (135), (040), (400), (331), (228), and (333), respectively. Upon the introduction of aluminum doping, a noticeable change in the pattern was observed. Specifically, a new secondary phase, $LaAlO_3$perovskite, emerged as a result of the aluminum doping process.

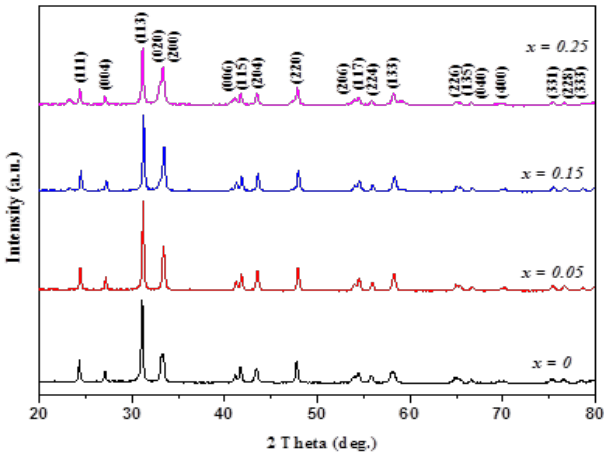

Fig. 1. XRD patterns of $La_{2-x}Al_xCuO_4$(x = 0.0, 0.05, 0.15, and 0.25) nanoparticles.

The production of a phase system, orthorhombic (La_2CuO_4) crystal structure following the substitution of La^{3+} by Al^{3+} ions demonstrates the creation of a composite. No complete phase transition has been seen besides the emergence of the extra phase Al_2O_3, La_2O_3, and CuO impurity phases are also not present. According to JCPDS card Nos. 82-0169, the La_2CuO_4 compounds have been indexed with the Cmca space groups, respectively [21,22].

The X-ray diffraction data were utilized to calculate the lattice parameters of the orthorhombic perovskite nanocomposites, employing equations (1) and (2).

$$\frac{1}{d^2} = \frac{h^2}{a^2} + \frac{k^2}{b^2} + \frac{l^2}{c^2} \tag{1}$$

where a, b, c, are the crystal lattice constants, and d is the inter-atomic distance. In Table 1, you can find the calculated lattice parameters a, b, and c, along with the unit cell volume (V), for both the cubic and orthorhombic perovskite phases. The variation in lattice parameters (as shown in Table 1) is attributed to the disparity in ionic radii between Al^{3+} and La^{3+} ions, as well as the influence of cation concentration in a solid solution on the miscibility limit of the corresponding phase formation.

Table 1. Sample code, crystallite size, lattice parameter, Rietveld refinement factors, and band gap values of $La_{2-x}Al_xCuO_4$ (x = 0.0, 0.05, 0.15, and 0.25) samples.

Sample	Sample code	Crystallite Size, L (nm)	Lattice Parameter, a, b & c (Å)	Fit Parameters	Energy gap (eV)
La_2CuO_4	a	54	5.835 5.838 13.149	R_{wp}= 6.39 R_p = 4.96 R_e = 5.84 S = 1.09	1.67
$La_{1.95}Al_{0.05}CuO_4$	b	50	5.831 5.834 13.145	R_{wp} = 6.72 R_p = 5.26 R_e = 5.98 S = 1.12	1.70
$La_{1.85}Al_{0.15}CuO_4$	c	45	5.826 5.829 13.138	R_{wp} = 7.70 R_p = 5.63 R_e = 5.93 S = 1.30	1.71
$La_{1.75}Al_{0.25}CuO_4$	d	41	5.819 5.822 13.135	R_{wp} = 9.96 R_p = 6.63 R_e = 5.69 S = 1.75	1.72

Aluminum incorporates into the La_2CuO_4 host lattice by occupying La^{3+} sites. The average crystallite size (D) was calculated using the Debye-Scherrer formula.

$$D = \frac{0.89\lambda}{\beta \cos\theta} \tag{2}$$

where, θ is the Bragg diffraction angle, λ is the X-ray wavelength, and β is the full width at half maximum (FWHM). The undoped La_2CuO_4 has an average crystallite size of about 41 nm, according to Table 1. La_2CuO_4 (orthorhombic) crystallite sizes between 41 and 54 nm respectively. The alterations in crystallite size for both La_2CuO_4 phases stem from the intricate interplay of atomic arrangements influencing grain growth. Preferential orientation along the facile direction during grain growth plays a pivotal role [23]. These fluctuations in crystallite dimensions are intricately linked to experimental factors like aluminum dopant concentration and intrinsic factors such as dopant nature and the crystal structure type, be it orthorhombic or cubic [24].

The Rietveld refinements carried out using the Fullprof software on the La_2CuO_4 are shown in Fig. 2. The improvements were made in order to validate two phase creation. The X-ray diffraction patterns of La_2CuO_4 nanoparticles, both observed and computed, exhibit a commendable agreement (Fig. 2). Additionally, the values listed in Table 1, approaching unity, indicate a close proximity of the observed and calculated 2θ values. The parameter 'S,' derived as the ratio Rwp/Re, where Rwp is the weighted profile and Re is the predicted weighted profile reliability factor, was employed to assess the goodness of fit. A 'S' value near unity validates that the refined parameters are estimated with high precision, suggesting an excellent goodness of fit.

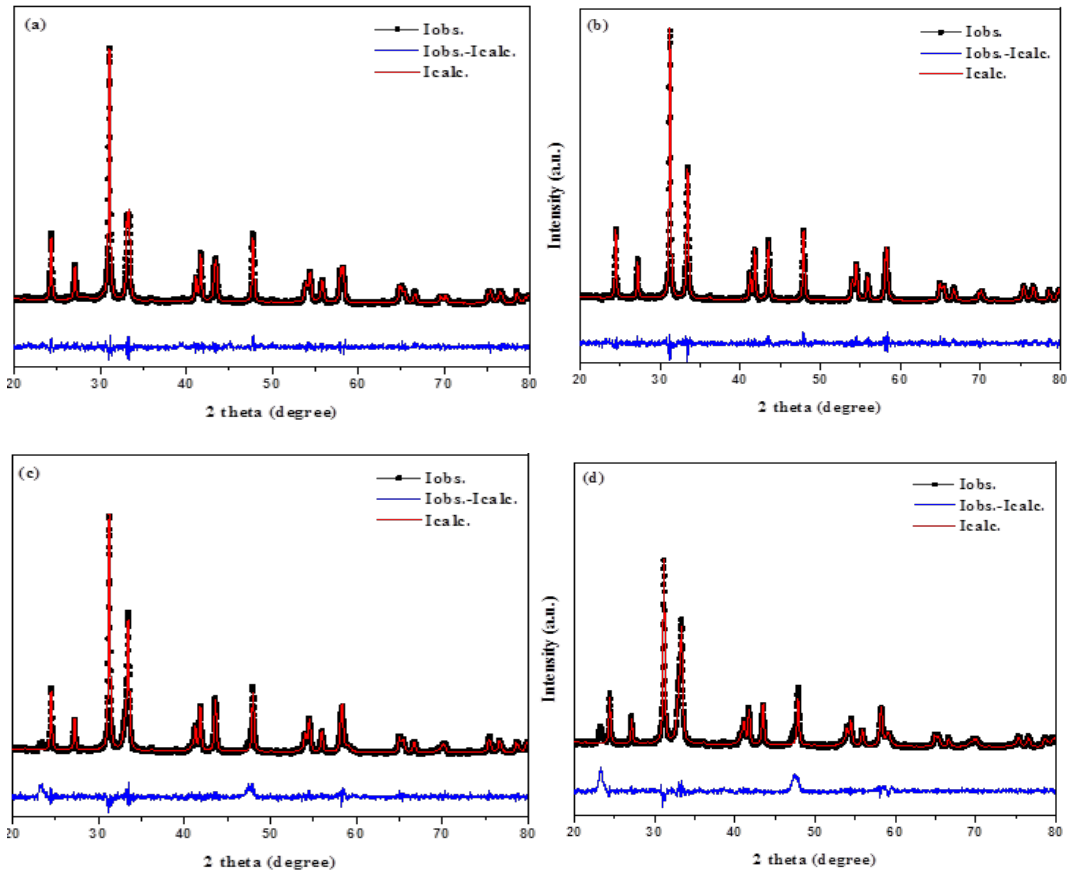

Fig. 2. Rietveld analysis of $La_{2-x}Al_xCuO_4$ *(x = 0.0, 0.05, 0.15, and 0.25) nanoparticles.*

3.2. FE-SEM and EDX analysis

The intra-granular pores in the La_2CuO_4 nanoparticles are visible in the FE-SEM micrographs of Fig. 3, during the pore structure are made of coalesced grains with identifiable grain boundary. Additionally, as aluminum concentration rises, bigger grains become smaller while intra-granular porosity rises. The La_2CuO_4 nanoparticles elemental composition was examined by EDX (Fig. 4), which proved the existence of La/Al, Cu, and O element. The accompanying inset table provides the respective proportions of the elemental composition.

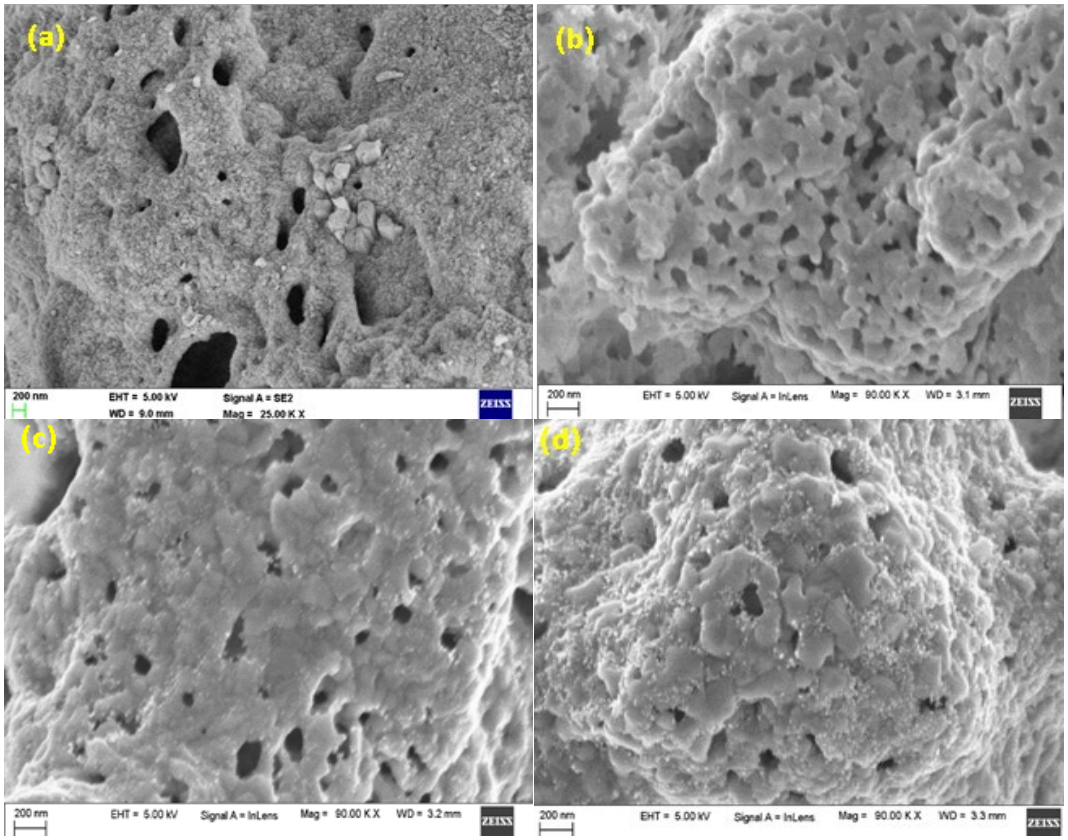

Fig. 3. FE-SEM images of $La_{2-x}Al_xCuO_4$(x = 0.0, 0.05, 0.15, and 0.25) nanoparticles.

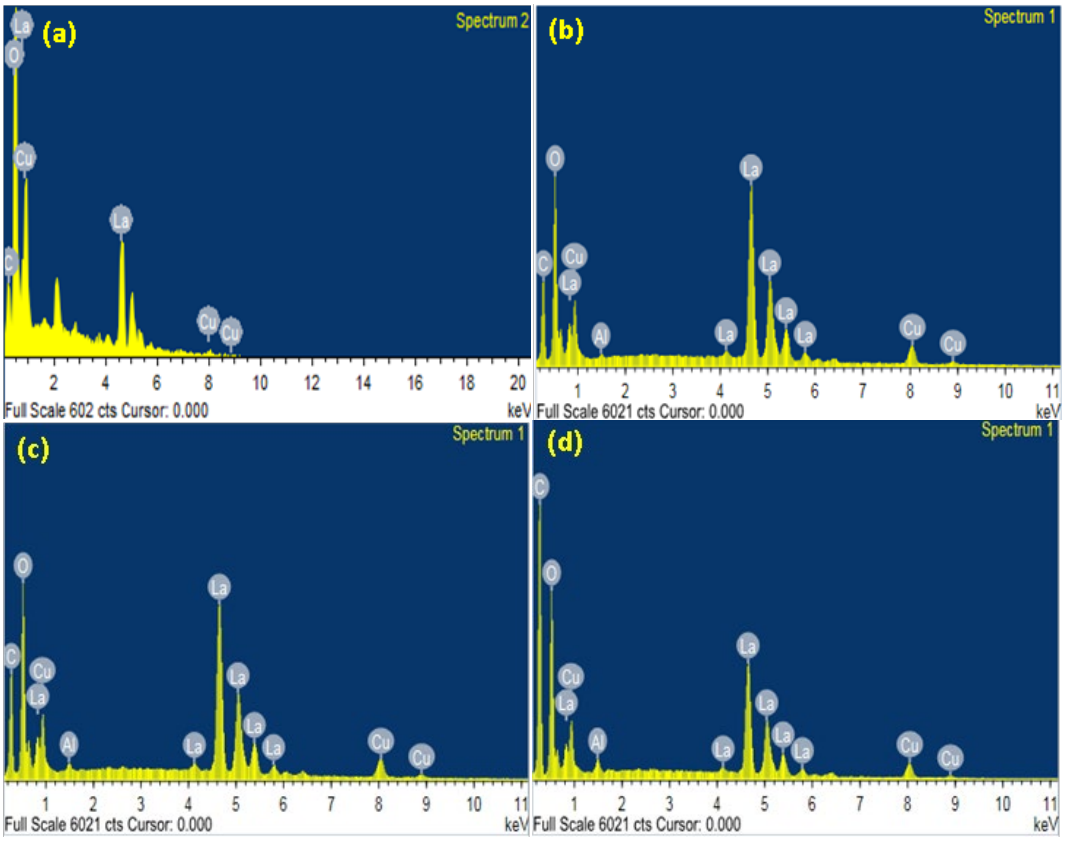

Fig. 4. EDX spectra of$La_{2-x}Al_xCuO_4$(x = 0.0, 0.05, 0.15, and 0.25) nanoparticles.

3.3. Optical properties

The room-temperature UV-visible diffuse reflectance spectra of the Al dopedLa_2CuO_4 system underwent analysis within the wavelength range spanning 200–800 nm, aiming to unveil its optical characteristics. Studies on diffuse reflectance are essential for determining the optical energy band gap. Using the updated Tauc relation provided by Eq. (3), it is calculated as follows [25]:

$$F(R)h\upsilon = A(h\upsilon - Eg)^n \tag{3}$$

Here, the symbols 'n' represent direct (n = 1/2) and indirect (n = 2) transitions, corresponding to direct and indirect band gaps. Typically, the Kubelka-Munk function [F(R)] is employed for the analysis of powder samples [26]. It transforms diffuse reflectance (R) into an equivalent absorption coefficient (α), as denoted by Equation (4):

$$\alpha = F(R) = \frac{(1-R)^2}{2R} \tag{4}$$

The values of direct band gap displayed in Fig. 5 are obtained by extrapolating the linear sections of a graph among $[F(R)h\upsilon]^2$ and hυ. For x = 0, 0.1, 0.3, and 0.5, respectively, the computed band gaps energies for the Al doped La_2CuO_4perovskite nanostructured system are 1.67, 1.70, 1.71, and 1.72 eV. Pure La_2CuO_4 has an energy band gap value of 1.67 eV, which is lower than the values of 1.88 eV and 1.24 eV reported in the literature [27].

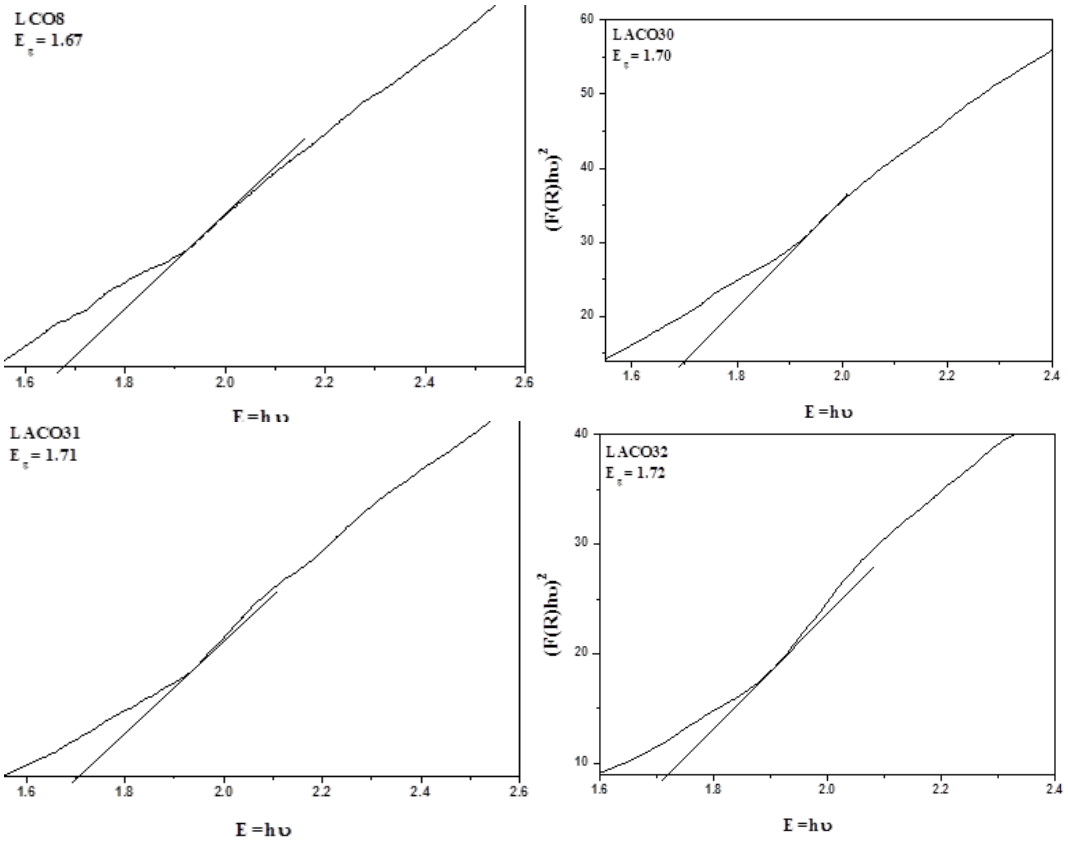

Fig. 5. (F(R) h)^{2}versus hυ plots for $La_{2-x}Al_xCuO_4$(x = 0.0, 0.05, 0.15, and 0.25) nanoparticles.

The manifestation of this phenomenon might be attributed to the effects of quantum confinement, particularly prevalent in the nano-scale domain. Due to the reduction in the ionic radius of La^{3+} compared to the host Al^{3+}(1.84 nm) upon aluminum doping, an effective substitution accentuates the bond-mismatch, particularly by constricting the $(LaO)_2$ layers [28]. It causes the CuO sheet to expand, which raises the band gap in the La_2CuO_4 system with Al doping.

3.4. FTIR analysis

The maturation of the perovskite architecture and the scrutiny of surface functional groups were appraised employing Fourier Transform Infrared (FTIR) spectroscopic analysis. The Al doped La_2CuO_4 system's Fourier transform infrared (FTIR) spectra were captured between 4000 and 400 cm^{-1} in Fig. 6. The vibrational stretching of O-H bonds in adsorbed water molecules can be associated with the broad spectral band peaking at around 3434 and 3750 cm^{-1}. This band might be a result of moisture's influence, which is less substantial for all samples, throughout the preparation of the sample for analysis [29]. The identification of a faint band in the range of 1184-1803 cm^{-1} can be ascribed to the presence of the O-O band. Additionally, a second subtle band at 2853 cm^{-1} may be associated with lingering nitrogen groups, stemming from the chosen combustion pathway during the synthesis of the materials [30]. At 434 cm^{-1} and 528 cm^{-1}, the CuO stretching mode band is seen. Additionally, the two bands at about 687 cm^{-1} and 1015 cm^{-1} are connected to the orthorhombic La_2CuO_4 phase's LaO and CuO stretching modes, which conform to the construction of the perovskite structure [31,32].

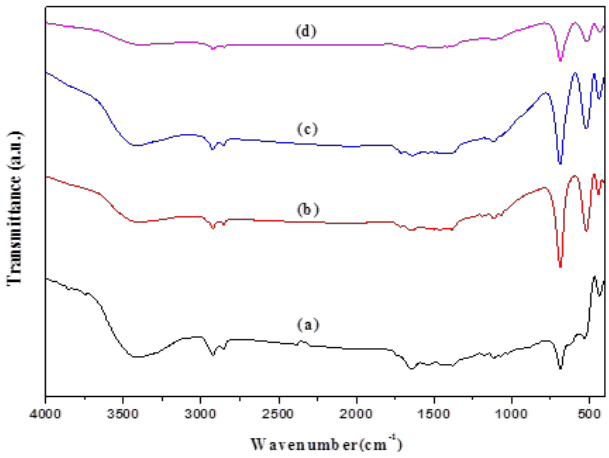

Fig. 6. FTIR spectra of $La_{2-x}Al_xCuO_4$(x = 0.0, 0.05, 0.15, and 0.25) nanoparticles.

3.5. Magnetic properties

The magnetic characterization of Al-doped La_2CuO_4 (x=0 to 0.25) is illustrated in Fig. 7, encompassing a magnetic field range spanning +15 kOe to -15 kOe. The M-H loops affirm the manifestation of ferromagnetic behavior at room temperature for $La_{2-x}Al_xCuO_4$ (x = 0 to 0.25), elucidated further in Table 2. The magnetic saturation (M_s) and remanent magnetization (M_r) values for the Al-doped La_2CuO_4 (x = 0 to 0.25) system range from 0.44 to 0.08 emu/g and 3.16 to 0.65 emu/g, respectively. The coercivity (H_c) values exhibit variation within the range of 21.22 to 133.42 Oe.

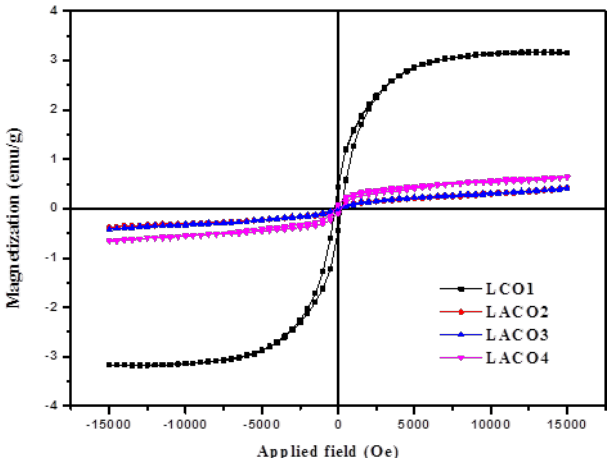

Fig. 7. Hysteresis loop of $La_{2-x}Al_xCuO_4$(x = 0.0, 0.05, 0.15, and 0.25) nanoparticles.

Table 2. Coercivity (H_c), Remanant magnetization (M_r) and Saturation magnetization (M_s) values of $La_{2-x}Al_xCuO_4$ (x = 0.0, 0.05, 0.15, and 0.25) nanoparticles.

Sample	Sample Code	H_c (O_e)	M_r (emu/g)	M_s (emu/g)
La_2CuO_4	LCO1	21.22	0.44	3.16
$La_{1.95}Al_{0.05}CuO_4$	LACO2	174.43	0.03	0.41
$La_{1.85}Al_{0.15}CuO_4$	LACO3	160.35	0.02	0.43
$La_{1.75}Al_{0.25}CuO_4$	LACO4	133.42	0.08	0.65

The profound alterations in M-H loops were scrutinized through the Al substitution in La_2CuO_4. Hence, shifts in magnetic attributes such as coercivity (H_c), saturation magnetization (M_s), and remanent magnetization (M_r) can yield valuable perspectives on the material's magnetic response [33]. Typically, the incorporation of impurities or dopant atoms has the capacity to exert an influence on the magnetic characteristics of a material. Certain dopants, such as aluminum ions, have the potential to elevate coercivity while concurrently diminishing the overall saturation magnetization. The escalation in coercivity implies an augmented difficulty in aligning or reversing magnetic domains within the material [34]. This phenomenon could stem from factors such as heightened magnetic anisotropy, the introduction of defects, or alterations in the crystal structure. As the reorientation of domains becomes more challenging, there is a potential decrease in the material's remanent magnetization (M_r). In this scenario, magnetic properties can be markedly affected by the size and shape of nanoparticles [35,36]. The concurrent increase in coercivity (H_c) alongside a reduction in saturation magnetization (M_s) and remanent magnetization (M_r) may suggest the material undergoing nanostructuring, potentially leading to quantum size effects or heightened surface effects [37]. The observed smaller crystalline size in the doped samples, compared to pure La_2CuO_4, indicates a higher proportion of surface atoms in the $La_{2-x}Al_xCuO_4$.

4. Conclusion

The synthesis of $La_{2-x}Al_xCuO_4$perovskite nanoparticles was accomplished through the microwave-assisted combustion method. The undoped La_2CuO_4 revealed a sole-phase perovskite characterized by an orthorhombic structure. The emergence of FT-IR bands at approximately 687 and 434 cm^{-1} is associated with the La/Al-O and Cu-O stretching modes of the orthorhombic La_2CuO_4 phase, affirming the perovskite structure. Concurrently, the optical bandgap witnessed a reduction from 1.67 to 1.72 eV, corresponding to the escalating Al^{3+} content from x = 0 to 0.25, respectively. The $La_{2-x}Al_xCuO_4$ (x = 0 to 0.25) samples exhibit the development of nanosized

crystallized grains, featuring porous structures and pore walls composed of fused grains. EDX analysis confirmed the presence of La, Al, Cu, and O elements. The $La_{2-x}Al_xCuO_4$ (x = 0 to 0.25) samples exhibit characteristics that make them potentially valuable in applications such as magnetic materials, catalysis, electronic devices, energy storage, sensors, and ceramics. The observed properties, including soft ferromagnetic behavior and unique structures, contribute to their versatility in various fields.

Acknowledgments

The authors (R. Jothiramalingam) extend his appreciation and acknowledgement to the financial support through Researchers Supporting Project number **(RSP2024R354),** King Saud university, Saudi Arabia.

References

[1] Allan, N. L., W. C. Mackrodt. Philosophical Magazine A 58, no. 4 (1988): 555-569; https://doi.org/10.1080/01418618808209937

[2] Puche, R. Saez, M. Norton, W. S. Glaunsinger, Materials Research Bulletin 17, no. 11 (1982): 1429-1435; https://doi.org/10.1016/0025-5408(82)90229-X

[3] Cabo-Bizet, Alejandro, Alejandro Cabo Montes de Oca. Physics Letters A 373, no. 21 (2009): 1865-1869; https://doi.org/10.1016/j.physleta.2009.03.018

[4] Longo, J. M., P. M. Raccah. Journal of Solid State Chemistry 6, no. 4 (1973): 526-531; https://doi.org/10.1016/S0022-4596(73)80010-6

[5] Mattheiss, L. F., Physical review letters 58, no. 10 (1987): 1028; https://doi.org/10.1103/PhysRevLett.58.1028

[6] Andraka, B., U. Ahlheim, J. S. Kim, G. Fraunberger, G. R. Stewart, B. Morosin, E. L. Venturini, D. S. Ginley, J. E. Schirber, Physical Review B 42, no. 16 (1990): 10016; https://doi.org/10.1103/PhysRevB.42.10016

[7] Czyżyk, M. T., G. A. Sawatzky, Physical Review B 49, no. 20 (1994): 14211; https://doi.org/10.1007/978-1-4757-9975-0_21

[8] Kwei, George H., A. C. Lawson, Mark Mostoller, Physica C: Superconductivity 175, no. 1-2 (1991): 135-142; https://doi.org/10.1016/0921-4534(91)90244-S

[9] Anderson, Philip W., Science 235, no. 4793 (1987): 1196-1198; https://doi.org/10.1126/science.235.4793.1196

[10] Fisk, Z., S. W. Cheong, D. C. Johnston, MRS bulletin 14, no. 1 (1989): 33-36; https://doi.org/10.1557/S0883769400053872

[11] Velasquez, Mauricio, Alexander Santamaria, Catherine Batiot-Dupeyrat, Applied Catalysis B: Environmental 160 (2014): 606-613; https://doi.org/10.1016/j.apcatb.2014.06.006

[12] Zhou, Xiaohua, Quanxi Cao, Ying Hu, Jinxiu Gao, Yulong Xu, Sensors and Actuators B: Chemical 77, no. 1-2 (2001): 443-446; https://doi.org/10.1016/S0925-4005(01)00721-3

[13] Tu, Q. Y., X. L. Chen, B. K. Ma, Z. X. Zhao, J. Q. Li, J. K. Liang, Physica C: Superconductivity 370, no. 2 (2002): 94-100; https://doi.org/10.1016/S0921-4534(01)00926-1

[14] Zhu, Junjiang, Zhen Zhao, Dehai Xiao, Jing Li, Xiangguang Yang, Yue Wu, Materials Chemistry and Physics 94, no. 2-3 (2005): 257-260; https://doi.org/10.1016/j.matchemphys.2005.04.041

[15] Tavana, Ali, Mohammad Akhavan, Claudia Draxl, Physica C: Superconductivity and its Applications 517 (2015): 20-25; https://doi.org/10.1016/j.physc.2015.07.001

[16] Dharmadhikari, Dipti V., Shrikant K. Nikam, Anjali A. Athawale, Journal of alloys and compounds 590 (2014): 486-493; https://doi.org/10.1016/j.jallcom.2013.12.141

[17] Li, Yifeng, Jianfeng Huang, Liyun Cao, Jianpeng Wu, Jie Fei, Materials characterization 64 (2012): 36-42; https://doi.org/10.1016/j.matchar.2011.11.015

[18] Bednorz, J. Georg, Masaaki Takashige, K. A. Müller, Materials research bulletin 22, no. 6 (1987): 819-827; https://doi.org/10.1016/0025-5408(87)90037-7
[19] Rahmani, Atefeh, JillaSaffari, Journal of Nanostructures 6, no. 4 (2016): 301-306.
[20] Chen, Hanxiao, Yin Xu, Kangmeng Zhu, Hui Zhang, Applied Catalysis B: Environmental 284 (2021): 119732; https://doi.org/10.1016/j.apcatb.2020.119732
[21] Sukumar, M., L. John Kennedy, J. Judith Vijaya, B. Al-Najar, M. Bououdina, Gopinath Mudhana, Vacuum 167 (2019): 407-415; https://doi.org/10.1016/j.vacuum.2019.06.036
[22] Longo, J. M., P. M. Raccah, Journal of Solid State Chemistry 6, no. 4 (1973): 526-531; https://doi.org/10.1016/S0022-4596(73)80010-6
[23] Yuvaraj, S., N. Manikandan, G. Vinitha, Photonics and Nanostructures-Fundamentals and Applications 45 (2021): 100922; https://doi.org/10.1016/j.photonics.2021.100922
[24] Chaillout, C., J. Chenavas, S. W. Cheong, Z. Fisk, M. Marezio, B. Morosin, J. E. Schirber, Physica C: Superconductivity 170, no. 1-2 (1990): 87-94; https://doi.org/10.1016/0921-4534(90)90233-5
[25] Yuvaraj, S., N. Manikandan, G. Vinitha, Ceramics International 44, no. 18 (2018): 22592-22600; https://doi.org/10.1016/j.ceramint.2018.09.033
[26] Li, Yifeng, Jianfeng Huang, Liyun Cao, Jianpeng Wu, Jie Fei, Materials characterization 64 (2012): 36-42; https://doi.org/10.1016/j.matchar.2011.11.015
[27] Enhessari, Morteza, Maryam Shaterian, Mohammad Javad Esfahani, Mohammad Nasser Motaharian, Materials Science in Semiconductor Processing 16, no. 6 (2013): 1517-1520; https://doi.org/10.1016/j.mssp.2013.05.005
[28] Häfliger, Petra S., Simon Gerber, R. Pramod, Vera I. Schnells, B. Dalla Piazza, Ralph Chati, V. Pomjakushin et al., Physical Review B 89, no. 8 (2014): 085113; https://doi.org/10.1103/PhysRevB.89.085113
[29] Hayat, Khizar, Falak Niaz, Shahid Ali, M. Javid Iqbal, M. Ajmal, M. Ali, Yaseen Iqbal, Sensors and Actuators B: Chemical 231 (2016): 102-109; https://doi.org/10.1016/j.snb.2016.02.127
[30] Sukumar, M., L. John Kennedy, J. Judith Vijaya, B. Al-Najar, M. Bououdina, Gopinath Mudhana, Vacuum 167 (2019): 407-415; https://doi.org/10.1016/j.vacuum.2019.06.036
[31] Whittingham, Alexander WH, Jordan Lau, Rodney DL Smith, Canadian Journal of Chemistry 99, no. 999 (2021): 773-779; https://doi.org/10.1139/cjc-2021-0059
[32] Al-Gunaid, Murad QA, Adel MN Saeed, Gayitri HM, Siddaramaiah Basavarajaiah, Polymer-Plastics Technology and Materials 59, no. 5 (2020): 469-483; https://doi.org/10.1080/25740881.2019.1669646
[33] Lees, S. T., I. Gameson, M. O. Jones, P. P. Edwards, M. Slaski, Chemistry of materials 10, no. 10 (1998): 3146-3155; https://doi.org/10.1021/cm9802752
[34] Ong, B. L., K. Jayaraman, C. Diao, T. J. Whitcher, A. Jain, H. Hung, M. B. H. Breese, E. S. Tok, A. Rusydi, Nature Communications 13, no. 1 (2022): 4639; https://doi.org/10.1038/s41467-022-31885-1
[35] Keimer, B., R. J. Birgeneau, A. Cassanho, Y. Endoh, M. Greven, M. A. Kastner, G. Shirane, Zeitschrift für Physik B Condensed Matter 91 (1993): 373-382; https://doi.org/10.1007/BF01344067
[36] Hu, Xiao, Aashish Sapkota, Vasile O. Garlea, Genda D. Gu, Igor A. Zaliznyak, John M. Tranquada, Physical Review B 107, no. 9 (2023): 094413; https://doi.org/10.1103/PhysRevB.107.094413
[37] Braicovich, Lucio, L. J. P. Ament, Valentina Bisogni, F. Forte, C. Aruta, G. Balestrino, N. B. Brookes et al., Physical review letters 102, no. 16 (2009): 167401; https://doi.org/10.1103/PhysRevLett.102.167401